Appendix I—Probability of Detection of Ground Rupture at Paleoseismic Sites

By Ray J. Weldon, II,[1] and Glenn P. Biasi[2]

Introduction

The generalized inversion (referred to here as the "Grand Inversion"; appendix N, this report) central to the Uniform California Earthquake Rupture Forecast, version 3 (UCERF3) for fault rupture probabilities includes a constraint term in which the rate of ground ruptures at paleoseismic sites is compared to the actual number observed from trenching and microgeologic study. This comparison is not a simple counting exercise for three reasons. First, not all earthquakes produce ground rupture. Second, the amount of slip in ground ruptures varies along the rupture so that with some probability slip could be small at the paleoseismic site and less likely to be detected. Third, preservation of evidence of ground rupture at a paleoseismic site is not guaranteed, and recognition of rupture in surviving evidence generally decreases with the age of the surface offset at the site as subsequent earthquakes accumulate.

This UCERF contribution addresses the probability of paleoseismic detection of ground rupture considering the effects of these three contributions. The results include a new method for combining these factors into a single probability of detection estimate. We include a table of probabilities for use in UCERF3 that is based on analysis of the Wrightwood, California, paleoseismic site. The original goal of this project was to develop a general framework so that site-specific probability of detection values could be estimated, but this proved to be too large a task for the time and resources allocated to UCERF3, so the values generated for Wrightwood were used for all sites.

Although we were not able to apply site-specific detection factors, some progress was made in identifying the parameters likely to make this task possible, so we include a discussion of what we consider to be crucial parameters in a supplement to this appendix (see "Supplement—A Possible Approach to Site-Dependent Probabilities of Detecting Ground Rupture at Paleoseismic Sites," which follows the References Cited) in the hope that our discussion will prove useful to future efforts. It is important to recognize that the approaches used by successive seismic hazard working groups evolve, and our threshold for changing an approach in UCERF3 relative to UCERF2 is whether the new approach is an improvement on the old, even if it is not yet perfect. In UCERF2, the number of prehistoric earthquakes recognized at a site was inferred to be equal to the number of earthquakes with surface rupture that include the site. This is clearly not the case because some paleo-earthquakes are not recorded at a site. Also, the preservation and subsequent recognition of prehistoric earthquakes are a function of the size of the earthquake and where the site is on the rupture, because ruptures taper

at their ends and have considerable spatial variability in their along-strike displacement. Although our approach is just the first step towards solving this problem, especially given that we apply the same detection filter to all sites, it certainly improves on the approach used in UCERF2, and hopefully the discussion we include as a supplement to this appendix will motivate even better approaches in UCERF4 and beyond.

We divide the problem (and this document) into two sections; the logical flow is sketched in figure I1. The "geology" section addresses how existing paleoseismic records can be understood in terms of the likely true number of events at the site. These probabilities depend on the frequency and type of layers deposited at the site and their deformation during earthquake rupture. These measures are, in general, site specific, but for UCERF3 are developed and explored using the paleoseismic record from the Wrightwood site. By applying these geologically motivated criteria, a probability of detection may be proposed as a function of displacement, and with it, an effective observed rate of ground rupturing earthquakes at the paleoseismic site. The "statistics" section starts from the opposite side with ruptures selected by the Grand Inversion (GI). Each rupture has a length and from that length a scaled average displacement. Given a representative degree of variability of surface displacement within a rupture and the location of a paleoseismic site within that rupture, each rupture has a displacement assigned at the site. The GI also gives the rates of occurrence of all ruptures affecting that site. By combining the gross predicted rate of ground ruptures with the probability of detection given displacement, a net paleoseismically detected rupture rate prediction is developed. The paleoseismically reported rate and its predicted rate, considering detectability, are compared within the GI to determine the quality of fit to the paleoseismic data at each site.
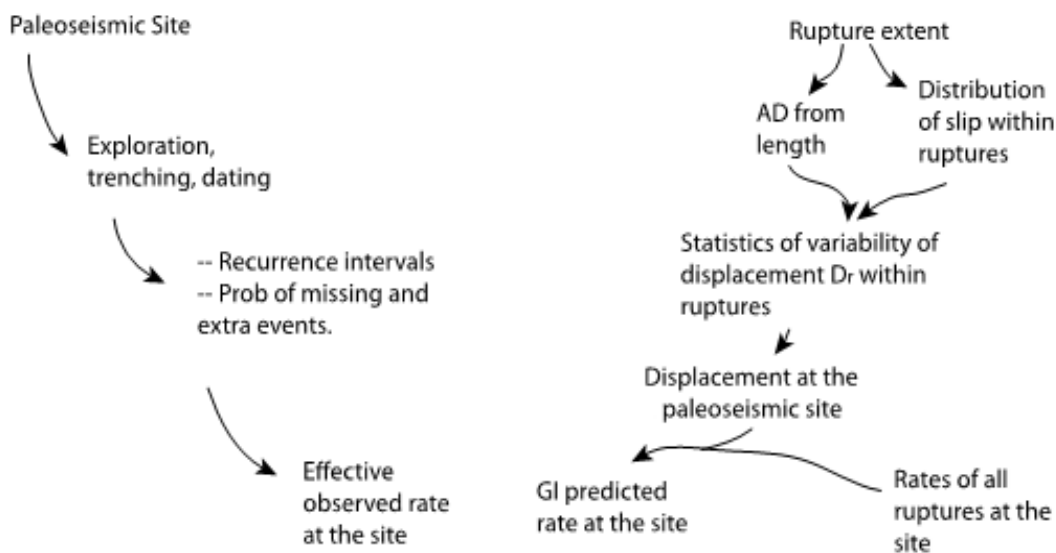

Figure I1. Flow chart for the geology (left side) and statistical (right side) elements for paleoseismic-event detection probabilities. AD, average displacement; Dr is specific displacement in a rupture; GI, Grand Inversion; prob., probability.

Geology

Earthquakes generate a wide variety of surface rupture features (fig. I2) that result in a wide range of expression of paleo-earthquakes in the geologic record. Geologic factors contributing to the reliability of data from paleoseismic studies have been examined by a number of workers, including McCalpin (1996), Seitz (1999), and Scharer and others (2007). Most of these studies have focused on the quality of individual observations; that is, how likely is it that a particular feature identified in a trench (usually referred to as an "event") is a prehistoric earthquake. Sometimes published results point out site uncertainties, like parts of the record that are inferred to be incomplete, but such information is rarely (if ever) incorporated into hazard uncertainty.

Figure I2. Photographs showing earthquake surface ruptures. Large earthquakes disrupt the ground surface in a wide variety ways, including cracks (fissures, upper left), folds (lower left) and "mole tracks" (right) that include a variety of lateral, compressional and extensional features all mixed together. The spatial variability of ruptures both in width and along strike requires multiple excavations to truly understand the paleo-earthquake. (Photographs of ruptures from the 1999 Izmit, Turkey, magnitude 7.4 earthquake, courtesy of T. Rockwell.)

For UCERF purposes the need is more precisely stated as the probability of detecting ground rupture at a paleoseismic site considering all site trenches and exposures; that is, what is the overall resolution of the site, not necessarily the quality of the evidence for individual earthquakes identified at the site. There is a general understanding that events can be missed if geologic layers are not deposited between distinct events. Discrete layers are not strictly required between events because fissures, scarp colluviums, and even offset of structures caused by an earlier earthquake can indicate an event within a stratigraphic hiatus (Weldon and others, 2002), but in general, the fundamental resolution of a site is strongly a function of the frequency of deposition of distinct, laterally traceable, and dateable stratigraphic layers. In practice other factors are also important, such as the number and spatial distribution of exposures, and the nature and width of the fault zone at the site. It is also true, although not as widely appreciated outside the paleoseismic community, that records can contain "events" that are not real earthquakes. This is due to the fact that some features can be interpreted in more than one way and because even real tectonic features cannot always be traced to the stratigraphic horizon that was at the ground surface during the event. For example, fractures terminating upward at different stratigraphic levels from a single earthquake can be misinterpreted as multiple events. The general solution to this problem is to have multiple exposures spread over a significant lateral extent of the fault to build up confidence that the real paleo-ground surface has been identified for each event and to identify spurious observations by their lack of consistency from exposure to exposure (for example, Scharer and others, 2007).

As discussed in greater detail in the supplement to this appendix, we infer that the following four criteria are the most important for defining a site's resolving power and propose a semiquantitative approach that can be used to compare or develop site-specific probabilities for resolving earthquakes at any site. The four criteria are: (1) spatial coverage—spatial extent of excavations/exposures both across and along the fault zone; (2) stratigraphic resolution—frequency of deposition of distinct layers at a site and the distribution of their thicknesses and lateral extents; (3) temporal resolution—number of datable units and the number of layers actually dated; and (4) structural-relief factor—fraction of the slip that is orthogonal to whatever records the offset, usually subhorizontal bedding.

At the Wrightwood paleoseismic site we can estimate the likelihood of recognizing ruptures with displacements of various sizes and evaluate what role the site criteria play in defining the likelihood because we have documented dozens of exposures over hundreds of meters of fault zone, dated hundreds of samples, and have a good idea of the ages and offsets of many earthquakes. Although we can see and routinely map fault displacements down to millimeters, the smallest offsets that we can carry from exposure to exposure and usually assign to a consistent stratigraphic horizon at Wrightwood are about 30 centimeters (cm). Figure I3 shows an example of a fault that decreases in displacement down to about 30 cm, at which point it becomes difficult to resolve and characterize. As discussed in greater detail in the appendix, 30 cm is also approximately the thickness of an average stratigraphic unit at the site. Thus, a 30 cm offset would find a thicker layer at the surface half the time and a thinner one the other half of the time (assuming each clastic layer sits at the surface about the same amount of time; more on this below). Because vertical separations locally equal the amount of slip at the site (the "structural relief" parameter has a value of 1; see for example figure I11 in the supplement to this appendix) there is about a 50-percent chance that a 30-cm offset will juxtapose two different stratigraphic units and thus provide clear evidence of an event. Similarly, a 1-meter (m) offset

will always juxtapose different stratigraphic units somewhere at the site because there are no units thicker than 1 m at this site.
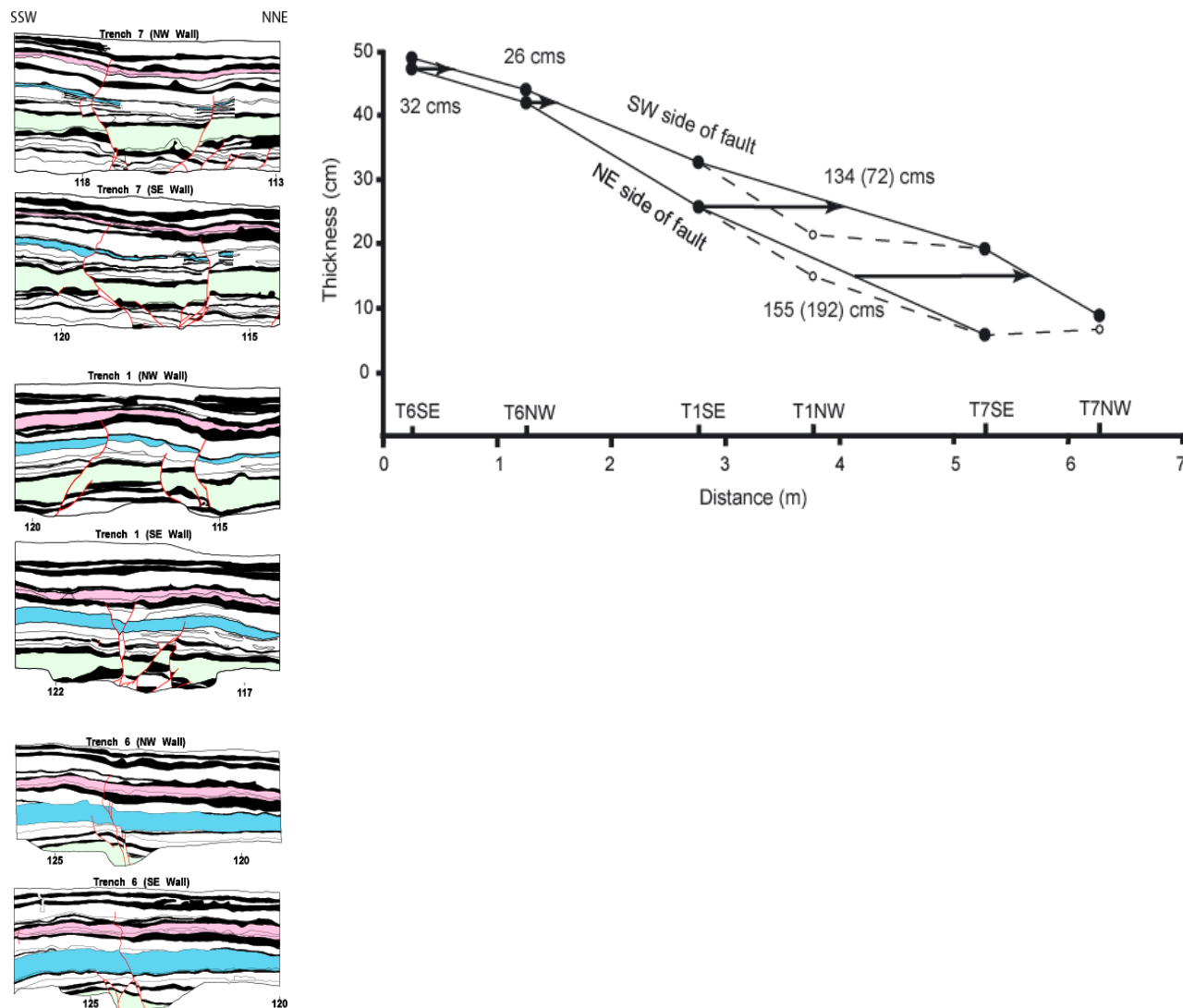

Figure I3. Three-dimensional trenching can be used to determine the slip on minor faults within a deforming zone, like the San Andreas fault at Wrightwood, California (Weldon and others, 1996). Note how the blue unit changes in thickness from northwest (NW) (top) to southeast (SE) (bottom) and across the fault that extends up to or above the pink layer. The plot above shows the resulting reconstruction of the right lateral component of the slip by matching the thickness of the blue unit across the fault. At the bottom (SE) the fault is at about the limit of the site's resolution, ~30 centimeters (cm), whereas at the top (NW) slip has increased to more than a meter and vertical separations (structural relief) and contrasts in unit thicknesses are very clear. Also note that sometimes the fault, caused by a single earthquake, can only be traced up to the pink layer but in other cases above it; this is a common problem with using upward termination alone, especially at sites without multiple closely spaced exposures. SSE, south-southeast; NNW, north-northwest.

This simple model is complicated by the fact that multiple earthquakes could occur while the same unit is at the ground surface. Thus, we need to consider not just the distribution in the thickness of units but how frequently they are laid across the Earth's surface. For the Wrightwood site we can see this information in figure I4. Although the rate of production of distinctive units varies considerably, on average for the site about 3 units are deposited between each earthquake. In spite of this, at least one earthquake (of 14 in the young part of the section) was missed in a long depositional hiatus (fig. I4).
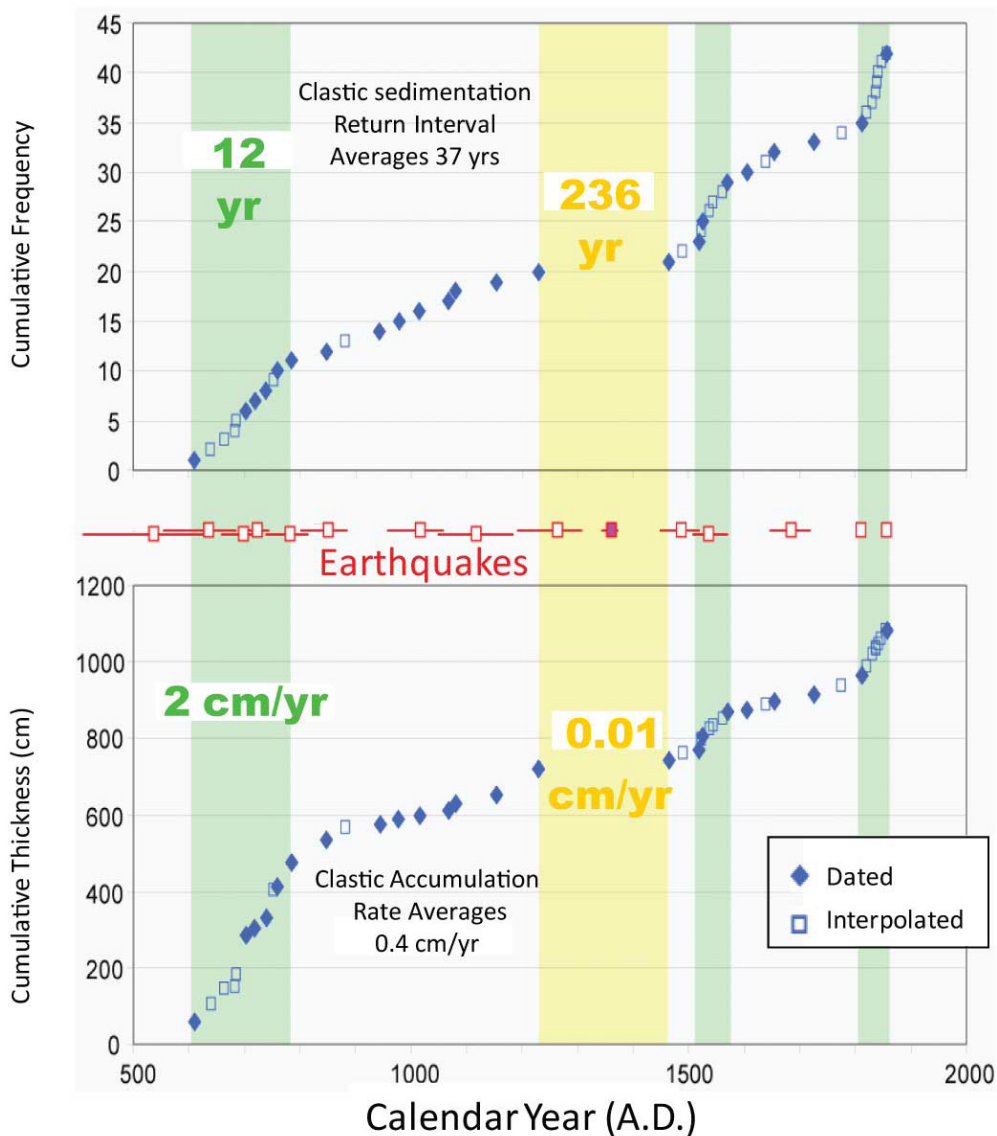

Figure I4. Plots of the frequency of clastic sedimentation events (upper) and accumulation rate of clastic units (lower) as a function of time for the upper section of the Wrightwood, California, paleoseismic site. The resolution of a site depends on the frequency and dateability of sedimentary units. In some parts of the record above, resolution approaches a decade; overall it averages 37 years. In slowly accumulating parts of the section, such as the 14th century, we infer that an event seen at adjacent sites (solid red square) was missed at this site (data from from Scharer, 2005; updated plots provided by K. Scharer). yr, years; cm, centimeters.

As discussed by Weldon and others (2004; and primary references therein), the missing event (PC-T, named after the same age event seen at sites to the north and south) is inferred to have had small displacement at Wrightwood (the total slip for W5 and the missing PC-T is about 1.4 m, so PC-T is likely to be a meter or less). In fact, the three other events (W1857, W3, W5) that were difficult to distinguish from subsequent or prior events all may have had a meter or less of slip (see table in Weldon and others, 2004); W1857 had approximately 1 m of slip; and because W3 ended in less than 26 km to the north (that is, before Pallett Creek), we infer it had a fraction of the ~7 m available for both W3 and 1812 (which was centered at Wrightwood and could have 4–6 m of slip). Similarly, the larger the displacement associated with an event, the larger the vertical separations seen in trenches, the greater juxtaposition of different stratigraphic units, and the thicker the associated growth strata (Weldon and others, 2002). This is consistent with the reasonable inference that small events are harder to see than large. Once displacement reaches 2 m at this site it would be difficult to miss the event, and it would be almost impossible to miss the largest displacments of 4–7 meters.

In summary, we believe that we can resolve about half of the paleo-earthquakes with 30 cm of displacement, three-fourths of events with approximately 1 m of slip (based on missing one of four events of this size), and essentially all paleo-earthquakes once the offset reaches 2 or more meters. We extrapolate these results to zero offset and put them in tabular form in table I1.

Table I1. Probability of detecting a rupture with given displacement at the Wrightwood, California, paleoseismic site.

[m, meters; P, probability]

Surface slip (m)	P(detection in trench)
0	0
0.10	0.05
0.20	0.25
0.30	0.50
1.00	0.75
2.00	0.95
4.00	0.99

By placing the data in this form we can combine it with the probability of different magnitude earthquakes rupturing the surface and the variability in displacement associated with ruptures to produce figure I5, the probability of surface rupture detection as a function of magnitude, as described in the next section. Effectively, the empirical shape of the probability of ground rupture as a function of magnitude is preserved, but the likelihood of seeing a given magnitude event is decreased systematically.

Finally, it is important to compare this admittedly imperfect approach to the alternatives, which are (1) to completely ignore the paleoseismic data because we don't fully understand its uncertainties or (2) to use it as if it is perfect, that is, assume it represents a perfect record of events at the site with no uncertainty beyond counting statistics (basically how it has been applied in past hazard analyses like UCERF2). Neither of these approaches seems preferred. We thus turn to the second branch of figure I1 and how the probabilities in table I1 can be used in a statistically forward sense to develop predicted observable rupture rates at paleoseisic sites.
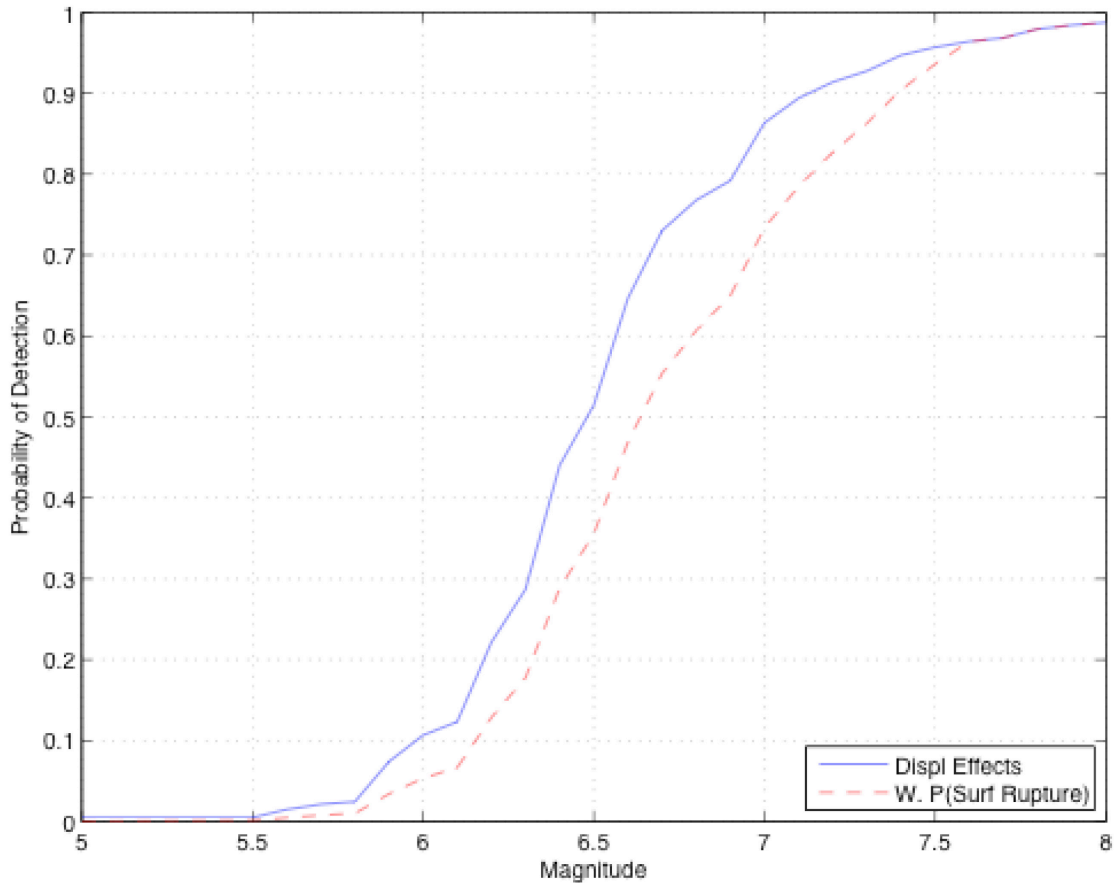
Figure I5.   Probability of surface rupture detection as a function of magnitude. Solid line shows the empirical probability of surface rupture from the compilation of Wells and Coppersmith (1993). The dashed line shows probabilities reduced by probabilities of detection from table I1. Displ, displacement; W. P(Surf Rupture), with reduced probability of surface rupture.

Statistics

The statistical approach starts from the opposite side of the problem (see flow chart figure I1) with ruptures selected by the Grand Inversion (GI). Each rupture has a length and from that length a scaled average displacement. Given a representative degree of variability of surface displacement within a rupture and the location of a paleoseismic site within that rupture, each rupture has a displacement assigned at the site. The GI also gives the rates of occurrence of all ruptures affecting that site.

Form of Required Probability Expressions

The GI assigns displacements D_{rj} to each rupture for each instance j that rupture is selected and becomes part of the final model. Each rupture is comprised of two or more fault

subsections. Each subsection extends in depth to the base of the seismogenic zone and has a length of half its depth. Expressing model results in terms of time, the model is "run" long enough that estimates of rates of each rupture are developed. The rates of all ruptures involving a given subsection are summed to become the rupture rate of that subsection. This inversion-predicted rate is compared with an observed paleoseismic rate, and the difference feeds back into the GI as a measure of the quality of fit of the inversion.

There is no guarantee in the GI that any specific rupture produces surface rupture. Thus, to compare predicted and observed surface rupture rates, conditional probabilities must be developed to reduce the total rupture rate to a prediction of the paleoseismically detectable rate considering imperfect preservation and trench coverage.

Trench Detection—Given slip at a paleoseismic site, $p_{td}(D)$ is the probability that displacement D will be reported as a surface rupture at the site. The form and values of $p_{td}(D)$ are empirically derived, based on the field investigation and site characteristics for evidence preservation described earlier in the "geology" section. Table I1 gives net values for $p_{td}(D)$ values summarizing experience from Wrightwood on the San Andreas Fault. In the future, site-specific probabilities of detection may be proposed and used in hazard analysis.

Surface Rupture Probability as a Function of Magnitude—The probability that an earthquake of a given magnitude produces surface rupture, $p_{sr}(M)$, was developed (fig. I5; Biasi and Weldon, 2006) from empirical data in Wells and Coppersmith (1993). For these data ground rupture is observed about half the time for ruptures of $M6.0$. The probability of ground rupture given magnitude depends on earthquake style, but the data are insufficient to make more detailed divisions and in California paleoseismic sites are concentrated on strike-slip faults. Event detection in trenches is a function of slip in meters, so a function $AD(M)$ is required to relate probability of event detection to magnitude. $AD(M)$ itself is discussed below. We write the net expression as $p_{sr}(M)$.

Trench Location—Surface ruptures typically have their largest displacements in the middle somewhere and taper to zero displacement at their ends. Thus, the probability of detection at a site for a given rupture depends on where the site is within the rupture. Small displacements at the ends of ruptures are more likely to be missed than large displacements in the middle. Relative location x within a rupture is indicated as x/L where L is the rupture length. Rupture profiles are assumed to be symmetric about $x/L=0.5$.

Natural Rupture Variability—In addition to tapering towards their ends, displacements also vary along strike in natural surface ruptures. As a way of synthesizing the variability of rupture displacements, surface rupture profiles are first normalized by length and average displacement. This step assumes that large and small ruptures have similar fractional variability (Hemphill-Haley and Weldon, 1999). The distribution of variability in rupture displacements, $p_{rv}(x)$, depends primarily on relative location x/L in the rupture. The number of available rupture profiles is only large enough to make representative variability plots for strike-slip style ruptures.

The probability of paleoseismic detection of a rupture with magnitude M by a site at location x within the rupture is:

$$p_{dt}(M, x)=p_{td}(D)p_{rv}(x)p_{sr}(M) ,\qquad\qquad(1)$$

where D is a function of $D_r(M)$ and x.

Method

Input data consist of rupture profiles from 21 strike-slip earthquakes from the collection of Wesnousky (2008). Rupture profiles from that work were normalized by length and by average displacement (*AD*). Rupture profiles in Wesnousky (2008) are regularly sampled, but differ in spacing and numbers of points, so for this work each contributing slip profile was resampled, generally at a greater density than the original data, and standardized onto a profile of 250 points. Each rupture and its reflection (because the direction of rupture is arbitrary) were included in the variability to remove the arbitrary direction of plotting. This effectively doubles the number of data in *x/L* bins for *x*<=0.5. The average of these normalized rupture shapes has been found to be well characterized by an analytic function, *sqrt(sin(pi×x/L))* (fig. I6, red line; Biasi and Weldon, 2006).
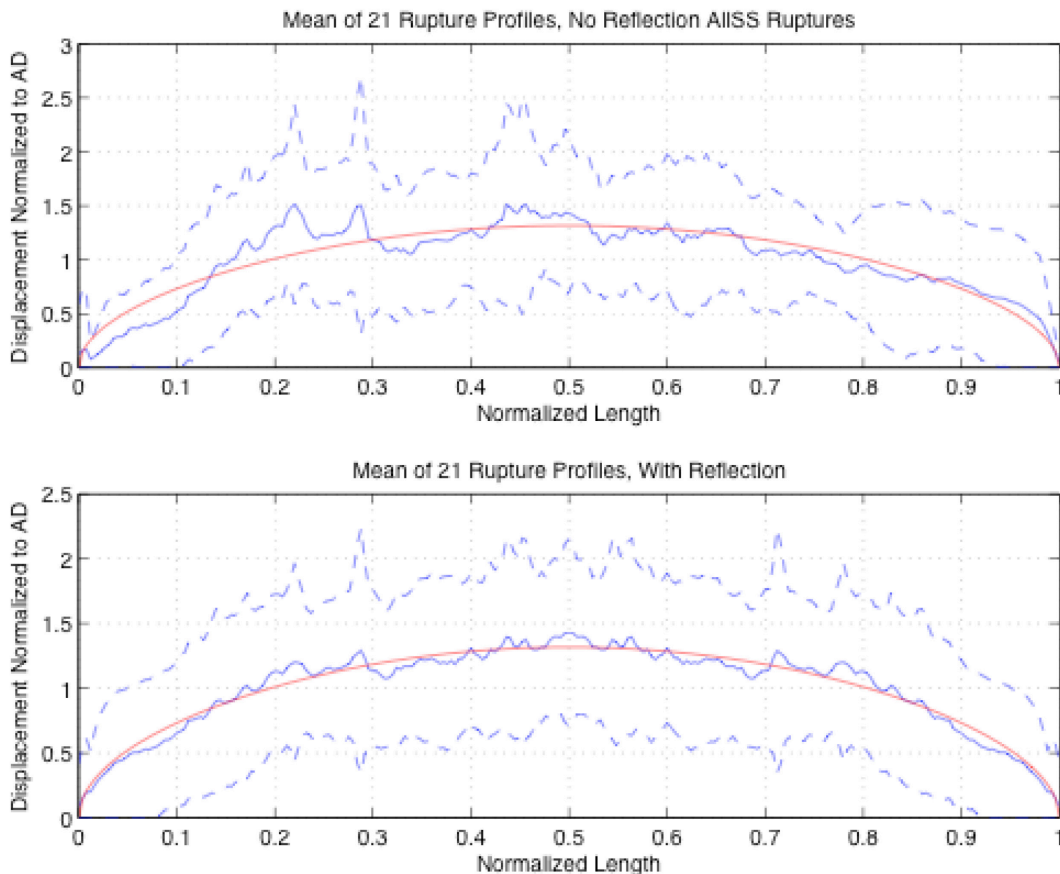

Figure I6. Rupture profile average and variability. Rupture profiles (along-strike measurements of offset) from 21 strike-slip earthquakes are used. Each profile is first normalized by length and average displacement, in meters. In the upper plot, each profile contributes once. In the lower plot, a second version of each profile is added after reflecting left to right. Dashed lines show one standard deviation ranges. *AD*, average displacement; AllSS, all strike-slip.

Figure I6 shows the variability *rv* around the mean shape. Variability depends on position within the normalized profiles in part because of the asymmetry of true displacement excursions (unbounded above, but cannot go below zero). Also, small offsets near the rupture ends are less likely to be reported in the literature, whereas larger ones are more likely to be noted. Figure I7 shows the variability of normalized displacements *d/AD* as a function of *x/L*. Values summarized in the histograms are gathered from ±2.5-percent widths to represent *d/AD* at points 5-percent apart over half the width of the distributions. Each histogram includes about 500 samples of *d/L*. Each histogram is thus an empirical estimate of variability of displacement, $p_{rv}(x)$. Using the normalized displacement data directly as p_{rv} proved unsuitable because the results were not robust to outliers. To develop more suitable $p_{rv}(x)$ probability-density functions, we took the central range (*AD*×1/3 to *AD*×2/3) of *d/AD* and use the log-normal distributions fit to them.
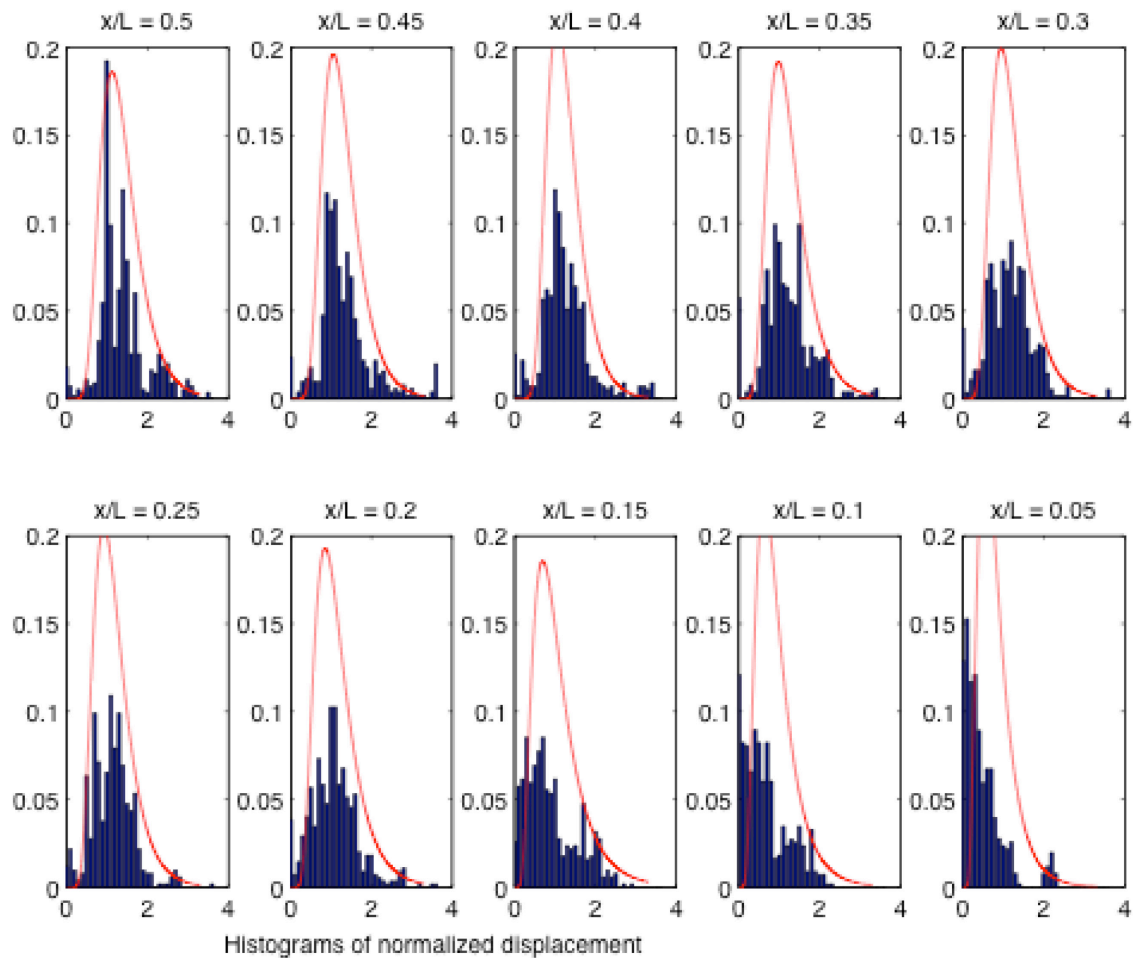

Figure I7.   Histograms of *d/AD* (normalized displacement) values at 10 locations *x/L*. Each histogram represents ~500 points. Bin widths in the histograms are 0.10 *d/AD* units. Lognormal models (red curves) were used to summarize variability.

To scale the normalized displacement distributions of $p_{rv}(x)$ to actual displacements, a relation of *AD* to *M* is required. Because paleoseismic detection probabilities will be applied to paleoseismic sites in California, we used *M-AD* data from California earthquakes (fig. I8). Moment magnitude (M_w) was used where available, and the geologic magnitude for the 1857, 1872, and 1906 earthquakes was also used. In figure I8, blue plus signs (+) are data, and red x points show the fit when magnitude is the dependent variable and *AD* is independent ($AD=2.32(M-6.12)$. Green circles assume *AD* is dependent and *M* is independent ($M=6.15+0.41AD$). The fits are quite similar. Why *AD* versus *M* should be linear is not clear; a similar plot of *M* versus *L*, not shown, is definitely not linear. Although admittedly empirical, this approach to *AD(M)* avoids more controversial magnitude-length and magnitude-area relations. Also in its favor is that results are not very sensitive to *AD(M)*. The linear regression for *AD(M)* predicts $AD=0$ for $M=6.12$. Slip below $M=6.20$ was linearly extrapolated to the smallest surface rupture average displacement of 0.007 m at M5.0. See table I2.

Probabilities $p_{td}(D)$ of seeing displacements in a trench (table I1) were linearly interpolated and applied to the *AD*-scaled log-normal model of displacements in figure I7. The sum over the full probability density function gives the probability of trench detection at location x/L. If surface rupture is assumed, result is the probability that it will be detected at a paleoseismic site at *x*. We then multiply by $p_{sr}(M)$ to obtain $p_{dt}(M, x)$.
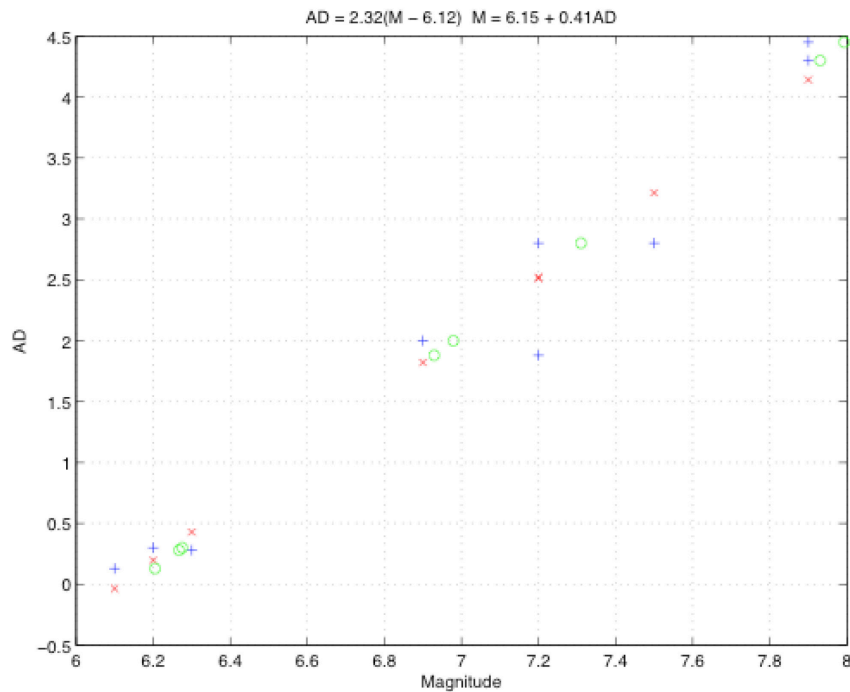
Figure I8. Magnitude (*M*) versus average displacement (*AD*) data used for *AD(M)*. *AD* and magnitude data (plus signs, +) are from Wesnousky (2008) and Biasi and others (appendix F, this report). Only ruptures from California earthquakes, plus the El Mayor-Cucapah, Baja Mexico, event were included. Red "x" and green "o" symbols are simple least-squares fits with magnitude and average displacement, respectively, as independent variables.

Figure I9 shows net probabilities that a ground rupture will be detected at a paleoseismic site as a function of earthquake magnitude and site location within the rupture. Lines with red stars are on whole magnitude units (5.0, 6.0, 7.0, 8.0). Unmarked red lines are on half-magnitude values. Intermediate detection of given magnitude (*dM*)=0.05 values are dashed. See table I2 for the corresponding numerical values. Entries reflect the combined effects of rupture variability as a function of location and the probability of producing ground rupture. Table I2 is intended as a look-up table for probabilities of observing the rupture in a trench site at some location *x*/*L*. For D_{sr} values or locations that fall between entries, extrapolation may be used to obtain final values. Displacements and probabilities of detection are 0 at *x*=0.
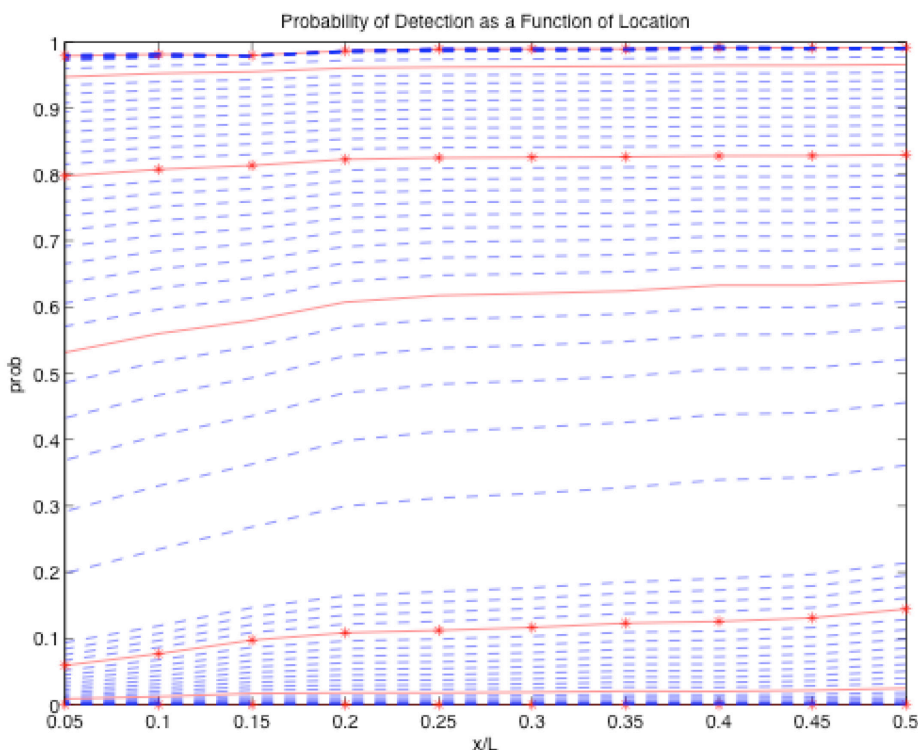

Figure I9.   Probability (prob) of paleoearthquake detection given magnitude and position (*x*/*L*) along a rupture. The plot shows the combined effects of the probability of event detection at a trench site and the probability of the earthquake having produced surface rupture. Lines with red stars are whole unit magnitudes (5.0, 6.0, 7.0, 8.0). Red lines are on half-magnitude values. Results on detection of given magnitude (*dM*)=0.05 intermediate magnitude steps are dashed. Magnitude (*M*), average displacement for given magnitude (*AD(M)*), and the probabilities are given in table I2.

Conclusions

Paleoseismic trenching data provide ground-truth estimates for likely frequency of ground-rupturing earthquakes. However, these estimates are imperfect, because not every earthquake affecting the site breaks the ground surface. Every earthquake that did break the surface at the site is not necessarily discovered because evidence may not be preserved, multiple

earthquakes may occur when the same layer is at the ground surface, and, more mundanely, trench locations may not be adequate to discover the necessary evidence. In addition, the potential for over-interpretation of the record can occur when a site investigation is perhaps incomplete and differing levels of upward disruption are construed as extra earthquakes. On the basis of analysis of opportunities for both of these miscounts of ground rupture at the thoroughly studied Wrightwood, California, site, we believe that paleoseismic studies are, on balance, unbiased estimators of earthquake occurrence, and hence, recurrence rate. A per site detection probability might be proposed in the future based on the exact circumstances of each paleoseismic site, but that is beyond our present scope.

The difference between the observed number of paleoseismic events and actual past earthquakes has been recognized in the paleoseismic community but not previously incorporated into California rupture forecasts. As a result, paleoseismic event data have been compared strictly to reported event rates in past hazard studies. This work presents a more robust explanation of the contributing elements of uncertainty in paleoseismic event rates, and a rough, empirically based method for including it in the Grand Inversion. Results are provided for probability of paleoseismic detection as a function of earthquake magnitude. The apparent recurrence rates developed by the Grand Inversion may be reduced by the probability values provided here to yield a predicted rate of paleoseismically observed events that can be compared to observations on an "apples-to-apples" basis.

Acknowledgments

Selected References

Akçiz, S., Ludwig Grant, L., and Arrowsmith, J.R., 2009, Revised dates of large earthquakes along the Carrizo section of the San Andreas fault, California, since A.D. 1310±30: Journal of Geophysical Research, v. 114, no. B01313.

Akciz, S., Grant, L., and Arrowsmith, R., 2006a, New and extended paleoseismological evidence for large earthquakes on the San Andreas fault at the Bidart Fan site, California [abs.]: Seismological Research Letters, v. 77, no. 2, p. 269.

Bakun, W.H., 2006, Estimating locations and magnitudes of earthquakes in southern California from modified Mercalli intensities: Bulletin of the Seismological Society America, v. 96, p. 1278–1295, doi:10.1785/0120050205.

Biasi, G.P., and Weldon, R.J., II, 2006, Estimating surface rupture length and magnitude of paleo-earthquakes from point measurements of rupture displacement: Bulletin of the Seismological Society America, v. 96, no. 5, p. 1612–1623.

Biasi, G., and Weldon, R.J., II, 2009, San Andreas fault rupture scenarios from multiple paleoseismic records—"Stringing pearls": Bulletin of the Seismological Society America, v. 99, no. 2A, p. 471–498.

Biasi, G.P., Weldon, R.J., II, Fumal, T.E., and Seitz, G.G., 2002, Paleoseismic event dating and the conditional probability of large earthquakes on the southern San Andreas fault, California: Bulletin of the Seismological Society America, v. 92, no. 7, p. 2761–2781.

Bronk Ramsey, C., 2009, Bayesian analysis of radiocarbon dates: Radiocarbon, v. 51, no. 1, p. 337–360.

Budding, K.E., Schwartz, D.P., and Oppenheimer, D.H., 1991, Slip rate, earthquake recurrence, and seismological potential of the Rodgers Creek fault zone, northern California: Geophysical Research Letters, v. 18, p. 447–450.

Dawson, T.E., McGill, S.F., and Rockwell, T.K., 2003, Irregular recurrence of paleoearthquakes along the central Garlock fault near El Paso Peaks, California: Journal of Geophysical Research, v. 108, doi:10.1029/2001JB001744.

Fumal, T.E., Weldon II, R.J., Biasi, G.P., Dawson, T.E., Seitz, G.G., Frost, W., and Schwartz D.P., 2002a, Evidence for large earthquakes on the San Andreas fault at the Wrightwood, California, Paleoseismic site—A.D. 500 to present: Bulletin of the Seismological Society America, v. 92, p. 2726–2760.

Fumal, T.E., Rymer, M.J., and Seitz, G.G., 2002b, Timing of large earthquakes since A.D. 800 on the Mission Creek strand of the San Andreas fault zone at Thousand Palms Oasis, near Palm Springs, California: Bulletin of the Seismological Society America, v. 92, no. 7, p. 2841–2860.

Goldfinger, C., Morey, A., Nelson, C.H., Gutiérrez-Pastor, J., Johnson, J.E., Karabanov, E., Chaytor, J., Eriksson, A., and the Shipboard Scientific Party, 2007, Rupture lengths and temporal history of significant earthquakes on the offshore and north coast segments of the Northern San Andreas fault based on turbidite stratigraphy: Earth and Planetary Science Letters, v. 254, no. 1, p. 9–27.

Grant, L.B., and Sieh, K., 1994, Paleoseismic evidence of clustered earthquakes on the San Andreas fault in the Carrizo Plain, California: Journal of Geophysical Research, v. 99, no. B4, p. 6819–6841.

Gurrola, L.D., and Rockwell, T.K., 1996, Timing and slip for prehistoric earthquakes on the Superstition Mountain fault, Imperial Valley, southern California, Journal of Geophysical Research, v. 101, no. B3, p. 5977–5985.

Hayward Fault Paleoearthquake Group (Lienkaemper, J.J., Schwartz, D.P., Kelson, K.I., Lettis, W.R., Simpson, G.D., Southon, J.R., Wanket, J.A., and Williams, P.L.), 1999, Timing of paleoearthquakes on the northern Hayward fault—Preliminary evidence in El Cerrito, California: U.S. Geological Survey Open-File Report 99–318, 34 p.

Hecker, S., Pantosti, D., Schwartz, D.P., Hamilton, J.C., Reidy, L.M., and Powers, T.J., 2005, The most recent large earthquake on the Rodgers Creek fault, San Francisco Bay area: Bulletin of the Seismological Society America, v. 95, no. 3, p. 844–860.

Hemphill-Haley, M.A., and Weldon, R.J., II, 1999, Estimating prehistoric earthquake magnitude from point measurements of surface rupture, Bulletin of the Seismological Society America, v. 89, p. 1264–1279.

Kelson, K.I., Simpson, G.D., Lettis, W.R., and Haraden, C.C., 1996, Holocene slip rate and recurrence of the northern Calaveras fault at Leyden Creek, eastern San Francisco Bay region: Journal of Geophysical Research, v. 101, no. B3, p. 5961–5975.

Kelson, K.I., Streig, A.R., and Koehler, R.D., 2006, Timing of late Holocene paleoearthquakes on the northern San Andreas fault at the Fort Ross Orchard site, Sonoma County, California: Bulletin of the Seismological Society America, v. 96, no. 3, p. 1012–1028.

Koehler, R.D., Witter, R.C., Simpson, G.D., Hemphill-Haley, E., and Lettis, W.R., 2004, Paleoseismic investigation of the northern San Gregornio fault at Pillar Point marsh near Half Moon Bay, California: U.S. Geological Survey National Earthquake Hazards Reduction Program, Final Technical Report, Award No. 02HQGR0071, 63 p., accessed August 9, 2013, at *http://earthquake.usgs.gov/research/external/reports/02HQGR0071.pdf.*

Lienkaemper, J.J., 2001, 1857 slip on the San Andreas fault southeast of Cholame, California: Bulletin of the Seismological Society America, v. 91, no. 6, p. 1659–1672, doi:10.1785/0120000043.

Lienkaemper, J.J., Williams, P.L., Dawson, T.E., Personius, S.F., Seitz, G.G., Heller, S., and Schwartz, D.P., 2003, Logs and data from trenches across the Hayward fault at Tyson's Lagoon (Tule Pond), Fremont, Alameda County, California: U.S. Geological Survey Open-File Report 03–488, 6 p., 8 plates, available at *http://pubs.usgs.gov/of/2003/of03-488/.*

Liu, J., Klinger, Y., Sieh, K., and Rubin C., 2004, Six similar sequential ruptures of the San Andreas fault, Carrizo Plain, California, Geology, v. 32, no. 8, p. 649–652.

McCalpin, J.P., 1996, Chapter 1—Introduction to paleoseismology, *in* McCalpin, J.P., ed., Paleoseismology, 2nd ed.: Elsevier Publishing, International Geophysics Series, v. 95, p. 1–32.

McGill, S.F., Dergham, S., Barton, K., Berney-Ficklin, T., Grant, D., Hartling, C., Hobart, K., Minnich, R. Rodriguez, M., Runnerstrom, E., Russell, J., Schmoker, K., Stumfall, M., Townsend J., and Williams J., 2002, Paleoseismology of the San Andreas fault at Plunge Creek, near San Bernardino, southern California: Bulletin of the Seismological Society America, v. 92, no. 7, p. 2803–2840, doi:10.1785/0120000607.

Middleton, T.J., 2006, Tectonic geomorphology of the southern Clark fault from Anza southeast to the San Felipe Hills—Implications of slip distribution for recent past earthquakes: San Diego State University, M.S. thesis, 109 p.

Patterson, A.C., and Rockwell, T.K., 1993, Paleoseismology of the Whittier fault based on 3-dimensional trenching at Olinda oil field, Orange County, southern California [abs.], Geological Society of America Abstracts with Programs, v. 25, no. 5, p. 131.

Rockwell, T.K., McElwain, R.S., Millman, D.E., and Lamar, D.L., 1986, Recurrent late Holocene faulting on the Glen Ivy North strand of the Elsinore fault at Glen Ivy marsh, *in* Ehlig, P.L., ed., Neotectonics and faulting in southern California, Geological Society of America, 82nd Annual Meeting of the Cordilleran Section, Guidebook and Volume, p. 167-175.

Rockwell, T., Seitz, G., Dawson, T., and Young, J., 2006, The long record of San Jacinto fault paleoearthquakes at Hog Lake—Implications for regional patterns of strain release in the southern San Andreas fault system [abs.], Seismological Research Letters, v. 77, p. 270.

Scharer, K.M., 2005, Earthquakes to mountains: fault behavior of the San Andreas fault and active tectonics of the Chinese Tian Shan: Eugene, University of Oregon, Ph.D. dissertation, 185 p.

Scharer, K.M., 2010, Changing views of the southern San Andreas fault: Science, v. 327, p. 1089.

Scharer, K.M., Biasi, G.P., and Weldon, R.J., II, 2011, A re-evaluation of the Pallett Creek earthquake chronology based on new AMS radiocarbon dates, San Andreas fault, California: Journal of Geophysical Research, v. 116, no. B12, doi:10.1029/2010JB008099.

Scharer, K.M., Biasi, G.P., Weldon, R.J., II, and Fumal, T.E., 2010, Quasi-periodic recurrence of large earthquakes on the southern San Andreas fault: Geology, v. 38, no. 6, p. 555–558.

Scharer, K.M., Weldon, R.J., II, Fumal, T.E., and Biasi, G.P., 2007, Paleoearthquakes on the southern San Andreas fault, Wrightwood, CA 3000 to 1500 B.C.—A new method for evaluating paleoseismic evidence and earthquake horizons: Bulletin of the Seismological Society America, v. 97, no. 4, p. 1054–1093.

Sieh, K.E., 1978, Prehistoric large earthquakes produced by slip on the San Andreas fault at Pallett Creek, California, Journal of Geophysical Research, v. 83, no. B8, p. 3907–3939.

Sieh, K.E., 1984, Lateral offset and revised dates of large prehistoric earthquakes at Pallett Creek, southern California: Journal of Geophysical Research, v. 89, no. B9, p. 7641–7670.

Sieh, K.E., 1986, Slip rate across the San Andreas fault and prehistoric earthquakes at Indio, California [abs.]: Eos (American Geophysical Union Transactions), v. 67, p. 1200.

Sieh, K., Stuiver, M., and Brillinger, D., 1989, A more precise chronology of earthquakes produced by the San Andreas fault in southern California: Journal of Geophysical Research, v. 94, no. B1, p. 603–623.

Seitz, G.G., 1999, The paleoseismology of the San Andreas fault at Pitman Canyon: Implication for fault behavior and paleoseismic methodology: Eugene, University of Oregon, Ph.D. dissertation, 278 p.

Seitz, G., Biasi, G., and Weldon, R., 1997, The Pitman Canyon paleoseismic record: a re-evaluation of San Andreas fault segmentation, *in* Hancock, P.L., and Michetti, A.M., eds., Paleoseismology—Understanding past earthquakes using Quaternary geology, Berlin, August 3–10, 1995: Journal of Geodynamics, v. 24, no. 1-4, p. 129–138.

Seitz, G., Biasi, G., and Weldon, R., 2000, An improved paleoseismic record of the San Andreas fault at Pitman Canyon, *in* Noller, J. S., and others, eds., Quaternary geochronology methods and applications: American Geophysical Union Reference Shelf 4, p. 563–566.

Simpson, G.D., Baldwin, J.N. Kelson, K.I., and Lettis, W.R., 1999, Late Holocene slip rate and earthquake history for the northern Calaveras fault at Welch Creek, eastern San Francisco Bay area, California: Bulletin of the Seismological Society America, v. 89, no. 5, p. 1250–1263.

Simpson, G.D., Thompson, S.C., Noller, J.S., and Lettis W.R., 1997, The northern San Gregorio fault zone—Evidence for the timing of late Holocene earthquakes near Seal Cove, California: Bulletin of the Seismological Society America, v. 87, no. 5, p. 1158–1170.

Sims, J.D., 1994, Stream channel offset and abandonment and a 200-year average recurrence interval of earthquakes on the San Andreas fault at Phelan Creeks, Carrizo Plain, California, *in* Prentice, C.S., Schwartz, D.P., and Yeats, R.S., eds., Proceedings of the workshop on paleoseismology: U.S. Geological Survey Open-File Report 94–568, p. 170–172.

Thatcher, W., Marshall, G., and Lisowski, M., 1997, Resolution of fault slip along the 470-km long rupture of the great 1906 San Francisco earthquake: Journal of Geophysical Research, v. 102, no. B3, p. 5353–5367.

Thorup, K.M., 1997, Paleoseismology of the central Elsinore fault in southern California--Results from three trench sites: San Diego State University, unpublished Master's thesis, 94 p.

Toppozada, T.R., Real, C.B., and Parke, D.L., 1981, Preparation of isoseismal maps and summaries of reported effects for pre-1900 California earthquakes: California Division of Mines and Geology Open-File Report 81-11 SAC, p. 172–174.

Vaughan, P.R., Thorup, K.M., and Rockwell, T.K., 1999, Paleoseismology of the Elsinore fault at Agua Tibia Mountain southern California: Bulletin of the Seismological Society America, v. 89, no. 6, p. 1447–1457.

Weldon, R.J., McCalpin, J.P., and Rockwell, T.K., 1996, Chapter 6—Paleoseismology in strike-slip tectonic environments, *in* McCalpin, J.P., ed., Paleoseismology, 2nd ed.: Elsevier Publishing, International Geophysics Series, v. 95, p. 271–330.

Weldon, R.J., II, Fumal, T.E., Powers, T., Pezzopane, S.K., Scharer, K.M., and Hamilton, J.C., 2002, Structure and earthquake offsets on the San Andreas fault at the Wrightwood, California paleoseismic site: Bulletin of the Seismological Society of America, v. 92, no. 7, p. 2704–2725.

Weldon, R., Scharer, K., Fumal, T., and Biasi, G., 2004, Wrightwood and the earthquake cycle—What the long recurrence record tells us about how faults work: Geological Society of America, GSA Today, v. 14, p. 4–10, doi:10.1130/1052-5173(2004)014.

Wells, D.L., and Coppersmith, K.L., 1993, Likelihood of surface rupture as a function of magnitude, Seismological Research Letters, v. 64, no. 1, p. 54.

Wells, D.L., and Coppersmith, K.J., 1994, New empirical relationships among magnitude, rupture length, rupture width, rupture area, and surface displacement, Seismological Society America Bulletin, v. 84, no. 4, p. 974–1002.

Wesnousky, S.G., 2008, Displacement and geometrical characteristics of earthquake surface ruptures: Issues and implications for seismic-hazard analysis and the process of earthquake rupture, Bulletin of the Seismological Society America, v. 98, no. 4, p. 1609–1632.

Working Group on California Earthquake Probabilities (Jackson, D.D., Aki, K., Cornell, C.A., Dieterich, J.H., Henyey, T.L., Mahdyiar, M., Schwartz, D., and Ward, S N.), 1995, Seismic hazards in southern California—Probable earthquakes, 1994–2024: Bulletin of the Seismological Society America, v. 85, 379–439.

Yu, E., and Segall, P., 1996, Slip in the 1868 Hayward earthquake from the analysis of historical triangulation data: Journal of Geophysical Research, v. 101, no. B7, p. 16101–16118.

Yule, D., Maloney, S., and Cummings, L.S., 2006, Using pollen to constrain the age of the youngest rupture of the San Andreas fault at San Gorgonio Pass [abs.]: Seismological Research Letters, v. 77, p. 245.

Zhang, H., Niemi, T., and Fumal, T., 2006, A 3000-year record of earthquakes on the northern San Andreas fault at the Vedanta marsh site, Olema, California [abs.]: Seismological Research Letters, v. 77, p. 176.

Table I2. Probability of paleoearthquake detection given magnitude and position along a rupture; values as plotted in figure I9.

[Column 1 is magnitude (*M*), and column 2 is average displacement given magnitude (*AD(M)*) from figure I8. Columns 3–12 are *x*/*L* fractions where *x* is the location within rupture length *L*]

M	AD(M)	0.5	0.45	0.4	0.35	0.3	0.25	0.2	0.15	0.1	0.05
5	0.0074	9.34E-06	6.68E-06	4.24E-06	6.98E-06	5.64E-06	4.88E-06	6.52E-06	8.28E-06	3.80E-06	1.74E-06
5.05	0.0148	0.0002	0.00018	0.00017	0.00016	0.00015	0.00014	0.00013	0.00012	8.46E-05	5.59E-05
5.1	0.0222	0.00053	0.00049	0.00047	0.00047	0.00044	0.00043	0.00042	0.00039	0.00029	0.000224
5.15	0.0296	0.00108	0.00098	0.00091	0.00095	0.00089	0.00086	0.00087	0.00085	0.00064	0.000504
5.2	0.0371	0.00205	0.00182	0.00167	0.00175	0.00164	0.00156	0.0016	0.0016	0.00118	0.00091
5.25	0.0445	0.00361	0.00316	0.00288	0.00303	0.00281	0.00267	0.00274	0.00273	0.001973	0.00149
5.3	0.0519	0.0059	0.00514	0.00469	0.00491	0.00453	0.0043	0.00439	0.00434	0.0031	0.0023
5.35	0.0593	0.00905	0.00788	0.00719	0.00749	0.00692	0.00655	0.00667	0.00651	0.004635	0.003398
5.4	0.0667	0.01318	0.01148	0.01051	0.01089	0.01006	0.00953	0.00964	0.00931	0.006638	0.004837
5.45	0.0741	0.01836	0.01604	0.01473	0.01516	0.01403	0.01329	0.01338	0.01278	0.009163	0.006664
5.5	0.0815	0.02465	0.02159	0.01992	0.020373	0.018889	0.017917	0.017937	0.016966	0.01225	0.008919
5.55	0.0889	0.032074	0.028188	0.026132	0.026541	0.024662	0.023421	0.023328	0.021869	0.01593	0.011635
5.6	0.0963	0.040606	0.03582	0.033365	0.033683	0.031369	0.029832	0.029575	0.027506	0.020224	0.014838
5.65	0.1038	0.050234	0.044483	0.041621	0.041791	0.039013	0.037154	0.036679	0.033876	0.025146	0.018548
5.7	0.1112	0.060925	0.054156	0.050882	0.050849	0.04758	0.045378	0.044629	0.040968	0.030701	0.02278
5.75	0.1186	0.072632	0.064804	0.061122	0.060828	0.057048	0.054486	0.053406	0.048767	0.036888	0.027541
5.8	0.126	0.085301	0.076386	0.072306	0.071691	0.067385	0.06445	0.062985	0.057249	0.043699	0.032836
5.85	0.1334	0.098872	0.088852	0.08439	0.083394	0.078554	0.075237	0.073331	0.066389	0.051122	0.038662
5.9	0.1408	0.113278	0.102149	0.097331	0.095889	0.090511	0.086806	0.084408	0.076156	0.059142	0.045015
5.95	0.1482	0.12845	0.116218	0.111072	0.109124	0.10321	0.099114	0.096174	0.086519	0.067739	0.051886
6	0.1556	0.144316	0.130997	0.125558	0.123044	0.1166	0.112114	0.108587	0.097443	0.076891	0.059264
6.05	0.163	0.160804	0.146423	0.140727	0.137592	0.130628	0.125757	0.1216	0.108893	0.086572	0.067134
6.1	0.1705	0.17784	0.162432	0.156516	0.152712	0.145242	0.139992	0.135168	0.120835	0.096757	0.075481
6.15	0.1779	0.195354	0.17896	0.172863	0.168348	0.160388	0.154767	0.149246	0.133232	0.107419	0.084286
6.2	0.1856	0.213758	0.196408	0.190171	0.184886	0.176448	0.17046	0.164191	0.146403	0.118851	0.093807
6.25	0.3016	0.361254	0.343196	0.339149	0.327713	0.318603	0.311795	0.299435	0.268145	0.234304	0.198183

M	AD(M)	0.5	0.45	0.4	0.35	0.3	0.25	0.2	0.15	0.1	0.05
6.3	0.4176	0.455718	0.440431	0.437848	0.425889	0.417975	0.411914	0.398259	0.362878	0.330137	0.291588
6.35	0.5336	0.520873	0.508123	0.506299	0.495344	0.488673	0.483495	0.470487	0.435608	0.40606	0.368926
6.4	0.6496	0.569704	0.559109	0.558004	0.547874	0.542288	0.537892	0.525877	0.493076	0.467021	0.432632
6.45	0.7656	0.608114	0.599491	0.599102	0.589651	0.585033	0.581334	0.570303	0.54003	0.517257	0.485934
6.5	0.8816	0.63939	0.632539	0.632673	0.624076	0.620311	0.617241	0.607209	0.579561	0.559729	0.531419
6.55	0.9976	0.665772	0.660406	0.660798	0.653289	0.650249	0.647728	0.638744	0.613696	0.596446	0.570963
6.6	1.1136	0.688848	0.684642	0.685079	0.678767	0.676314	0.674254	0.666343	0.643805	0.628791	0.605907
6.65	1.2296	0.709709	0.706358	0.706716	0.701557	0.69956	0.697872	0.691009	0.670839	0.657744	0.637216
6.7	1.3456	0.729067	0.726321	0.726547	0.7224	0.720747	0.719348	0.71346	0.695478	0.684014	0.665602
6.75	1.4616	0.747372	0.745041	0.745129	0.741812	0.740411	0.739233	0.734212	0.718214	0.708129	0.691602
6.8	1.5776	0.764904	0.762849	0.762817	0.760147	0.758929	0.757914	0.75364	0.739412	0.730486	0.715628
6.85	1.6936	0.781831	0.779959	0.779829	0.777648	0.776559	0.775664	0.772016	0.759344	0.751389	0.738
6.9	1.8096	0.798257	0.796502	0.796299	0.794476	0.793478	0.79267	0.789536	0.778216	0.771075	0.758971
6.95	1.9256	0.814243	0.812565	0.812309	0.810742	0.809808	0.809063	0.806342	0.796186	0.789726	0.778743
7	2.0416	0.829827	0.828198	0.827908	0.826518	0.82563	0.82493	0.822537	0.813372	0.807485	0.797478
7.05	2.1576	0.84503	0.843435	0.843125	0.841855	0.841	0.840332	0.838195	0.829868	0.824465	0.815304
7.1	2.2736	0.859868	0.858297	0.857977	0.856784	0.855953	0.85531	0.853369	0.845743	0.840754	0.832328
7.15	2.3896	0.874347	0.872796	0.872476	0.871329	0.870517	0.869891	0.8681	0.861054	0.856424	0.848636
7.2	2.5056	0.888474	0.886941	0.886627	0.885503	0.884707	0.884096	0.882414	0.875841	0.87153	0.864295
7.25	2.6216	0.902251	0.900737	0.900434	0.899316	0.898536	0.897936	0.896333	0.890139	0.886116	0.879364
7.3	2.7376	0.915679	0.914186	0.913899	0.912776	0.912011	0.911421	0.90987	0.903971	0.900217	0.893888
7.35	2.8536	0.928761	0.927291	0.927023	0.925885	0.925136	0.924557	0.923035	0.917357	0.913862	0.907905
7.4	2.9696	0.941495	0.940053	0.939807	0.938646	0.937915	0.937348	0.935835	0.93031	0.927071	0.921446
7.45	3.0856	0.953881	0.952472	0.952253	0.95106	0.95035	0.949794	0.948274	0.942841	0.939863	0.934537
7.5	3.2016	0.965918	0.964547	0.964359	0.963126	0.962441	0.961899	0.960354	0.954957	0.952252	0.947198
7.55	3.3176	0.977603	0.976277	0.976126	0.974843	0.974188	0.973661	0.972075	0.966663	0.964247	0.959446
7.6	3.4336	0.988935	0.987662	0.987555	0.986209	0.985588	0.98508	0.983436	0.97796	0.975856	0.971294
7.65	3.5496	0.9895	0.988302	0.98825	0.98684	0.986268	0.985786	0.984085	0.978559	0.976812	0.972525
7.7	3.6656	0.989995	0.988883	0.988894	0.987404	0.986886	0.986435	0.984659	0.979041	0.977673	0.973652

M	AD(M)	0.5	0.45	0.4	0.35	0.3	0.25	0.2	0.15	0.1	0.05
7.75	3.7816	0.990417	0.989401	0.989489	0.987899	0.987443	0.987025	0.985158	0.979409	0.978448	0.974685
7.8	3.8976	0.990762	0.989856	0.990035	0.988322	0.987937	0.987557	0.985579	0.979665	0.979139	0.975634
7.85	4.0136	0.991023	0.990244	0.990531	0.98867	0.988366	0.988028	0.985921	0.979811	0.979752	0.976505
7.9	4.1296	0.991195	0.990561	0.990976	0.988939	0.988726	0.988437	0.986181	0.979846	0.980288	0.977306
7.95	4.2456	0.99127	0.990803	0.99137	0.989124	0.989015	0.988781	0.986356	0.97977	0.98075	0.978041
8	4.3616	0.991239	0.990964	0.991708	0.98922	0.989228	0.989056	0.986441	0.979583	0.981138	0.978713
8.05	4.4776	0.991095	0.991038	0.991987	0.989222	0.989362	0.989259	0.986434	0.979285	0.981453	0.979325
8.1	4.5936	0.990827	0.991019	0.992204	0.989123	0.98941	0.989386	0.98633	0.978874	0.981695	0.97988
8.15	4.7096	0.990424	0.990899	0.992354	0.988917	0.989369	0.989432	0.986124	0.978349	0.981863	0.98038
8.2	4.8256	0.989876	0.99067	0.99243	0.988598	0.989231	0.989392	0.985813	0.97771	0.981959	0.980826

Supplement—A Possible Approach to Site-Dependent Probabilities of Detecting Ground Rupture at Paleoseismic Sites

Early in UCERF3 it was hoped that we could develop a site-specific set of probabilities of detecting ground rupture. To do so in a practical manner that could be applied to the dozens of sites used by UCERF3 would require developing a set of parameters that could be estimated at each site, generally from available records that often include selected trench logs (vertical maps of trench exposures), a stratigraphic column, available age control, and a map of excavaions (or exposures). This appendix summarizes some of our thoughts and a very preliminary approach to semiquantitatively assess and compare the probabilities of detecting ground rupture at diferent sites. Although it was not possible to complete this goal for UCERF3, we hope this will help guide or inspire future efforts.

Spatial Coverage

The spatial extent of trenches or other excavations that provide exposures both across and along a fault zone is crucial for determining the likelihood that earthquakes could be missed at the site. Clearly the excavations need to span the active fault zone, which can be as little as a meter to hundreds of meters wide (for example, ~175 m at Wrightwood, California). With modern imagery (especially lidar) it is relatively easy to assess what fraction of the active zone has been spanned. Because surface ruptures are so variable (fig. I2), it is more difficult to assess how many cross-fault exposures are necessary, or equivalently how much along-strike coverage is required to expose all earthquakes. An informal survey of completely developed paleoseismic sites suggests that between one and three exposures per earthquake recognized, or a lateral extent comparable or greater than the width of the fault zone, are required. Obviously, some trenches fortuitously reveal clear evidence for multiple events and others reveal no event evidence, and may not even cross the fault, but on average, if one interprets more events than exposures, one is unlikely to fully understand the deformation or the true number of events. Thus, we assign a rating of 0 to 1 corresponding to the fraction of trench coverage compared to that required to span the zone and recognize the number of events advocated. At Wrightwood this factor is 1 for the upper section used in UCERF3.

Stratigraphic Resolution

The frequency of deposition of distinct layers at a site and the distribution of their thicknesses and lateral extents provide key measures of a site's resolution. Sites with many distinctive and dateable units provide the opportunity to separate earthquakes stratigraphically, correlate event evidence from exposure to exposure, and, if layers are dateable, determine the age of the events. Essential for our approach here is the observation that displacements become harder and harder to observe and distinguish from one another as the stratigraphic units become thicker and less distinctive. For example a 20-cm displacement is easy to see in centimeter-thick layers but hard to see in more massive, meter-thick layers. Additionally, if all the layers look the same, it is difficult to recognize a contrast when different layers are juxtaposed by deformation.

For example, imagine an offset of a few centimeters cutting up through the section shown in figure I10; it would be recognizable in the fine laminated black and white units just above the lower string, but likely not recognizable in either the massive grey material below or the debris above these thin, distinctive layers. From a practical point of view if the offset is greater than the

bed thickness it terminates within, it is likely to be seen, and by contrast if it is less than the bed thickness it is not. The distinctiveness of the layers, sharpness of contacts, and factors other than simply thickness certainly affect one's ability to see offset or folding. However, these factors generally determine how finely a stratigraphic section can be subdivided and thus are captured, at least to some extent, by the thickness of layers. Although some features associated with earthquakes can be recognized despite the unit thickness, we will take slip compared to layer thickness as a more reliable general rule to assess the relative resolution of a site.

Figure I10. Photograph of a 50-centimeter-thick part of the ~20-meter section at the Wrightwood, California, paleoseismic site. Coarse central unit is a debris flow, thin dark layers are peats or soils, and thin light-colored units are eolian or distal facies of debris flows or overbank fluvial deposits. Fundamentally, a site's ability to provide paleoseismic data depends on the number, thickness, organic content (for carbon-14 (^{14}C) dating), and frequency of emplacement of sedimentary units that cover the surface rupture of the earthquake. (Photograph by K. Scharer, USGS.)

If we know the distribution of stratigraphic unit thicknesses at a site, we can develop a probability function for how likely it is that a rupture of a particular size will find a unit more or less thick than its offset at the ground surface. For example, at the Wrightwood paleoseismic site the average layer thickness is approximate 30 cm. Thus, a 30-cm offset would find a thicker layer at the surface half the time and a thinner one the other half of the time (assuming each clastic layer sits at the surface about the same amount of time; more on this below). Thus with our simple rule we can conclude that a 30-cm offset would be seen about 50 percent of the time, and a 1 m offset essentially all of the time because there are no units thicker than that at this site.

Temporal Resolution

Many authors have discussed temporal resolution (for example, McCalpin, 1996), so we do not discuss it here beyond noting that a common goal is twice as many dated units as

earthquakes (one date directly above and one directly below). Ideally, all datable units should be dated because simply focusing on the event horizon may not permit one to recognize hiatuses in the stratigraphy (for example, fig. I4) and statistical approaches (for example, Biasi and Weldon, 1996; Bronk Ramsey, 2009) provide greater precision for individual dates as more dates are included in an ordered sequence. For our current purposes, there needs to be adequate dating to determine the frequency of sedimentation events relative to the recurrence interval. To assess the temporal resolution of a site one can define a simple ratio of dated layers to interpreted events. At the Wrightwood site (upper section) it is 23/12 (2 of the 14 events are historic and thus not dated), approximately our goal of 2:1. Note that total number of samples or dates may not be a good measure of resolution if many or all samples are in one or a few layers. The key is the number of dated layers, relative to events interpreted.

Structural-Relief Factor

So far we have not considered that the slip in an earthquake-faulting event might not be perpendicular to the stratigraphy that is recording the offset. Clearly slip that is not perpendicular to bedding will be harder to recognize, because it does not separate stratigraphic units as much as the same amount of slip that is perpendicular to layers. Thus, we define a structural relief factor that converts the slip to vertical separation. In this context, we define structural relief as the sum of all vertical separations across all individual faults and folds, just as one calculates the total relief associated with a hike or bicycle trip as the sum of all relief traversed, not the net relief or difference between the beginning and end. This is illustrated in figure I11.
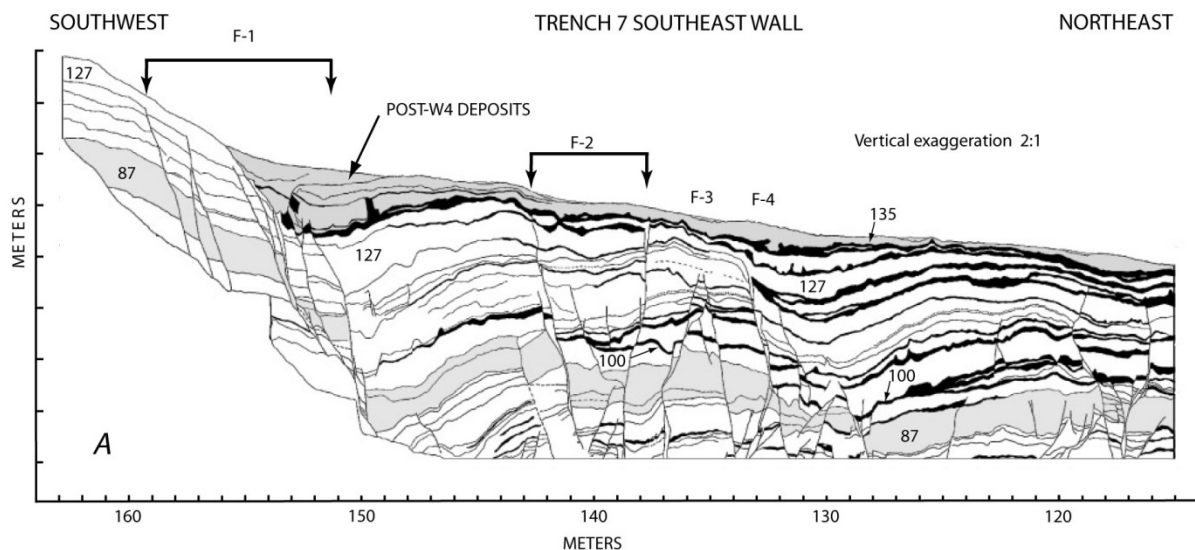

Figure I11. Deformation produced by ~15 meters of oblique right-normal slip since the lowest completely exposed layer (unit 87). Structural relief, the sum of all the vertical separations across all individual faults and folds, is ~12 m, approximately the total slip across this secondary structure in the San Andreas Fault Zone at Wrightwood (figure from Fumal and others, 2002a; see Weldon and others, 2002 for offset discussion). F1, F2, and so on are fault zones discussed in the context of the original figure. W4, is Wrightwood, California, paleo-earthquake 4.

In concept, if the marker (like bedding) is flat, this would result in a value of 1 for a vertical dip slip fault, where slip is perpendicular to the flat bedding and 0 for a pure strike-slip fault. However, most faults are not purely dip slip or strike slip, and most bedding is not perfectly flat. In addition, many strike-slip paleoseismic sites are located on step-overs or other structurally complex sites that produce secondary faulting and folding that often generates structural relief. By looking at cross sections through paleoseismic sites, we can define this factor, at least to a general degree, for each site.

Structural relief, as used here can also be caused by laterally offsetting layers that dip or change thickness in the direction of slip. A good example of this can be seen in figure I3. Offsets down to about 30 cm, about the threshold of resolution at the Wrightwood site, were resolved by comparing thickness changes in layers across small secondary faults.

Hypothetical Procedure

With the following four components we could make a simple model to assess the likelihood that a particular displacement will be recognized at the site:

Estimate spatial coverage from site maps and (or) geomorphic expression on a scale of 0 to 1. A value of 1 means the investigation spans the entire zone and has enough exposures along the fault to adequately expose evidence for the claimed number of intervals. A 0.5 would mean either half the likely fault zone was crossed, but with adequate coverage to resolve events, or the entire zone was crossed, but with inadequate along-fault coverage. Multiply all probabilities determined below by this factor; that is, reduce the individual probabilities by the likelihood that the event misses the trench network.

Calculate the structural relief factor from trench logs across the fault zone on a scale of 0 to 1+ where 1 is the actual slip amount. Note that there can be greater structural relief than the net offset (imagine a normal fault offset with a synthetic or conjugate secondary structure forming a graben along the fault trace).

Estimate the stratigraphic resolution using the distribution of different thickness units that can be determined from published stratigraphic columns or, if available, measured off trench logs for the site. Determine the average number of units deposited between earthquakes identified and combine unit thicknesses if needed to estimate the amount of stratigraphy between each average interval. Assume that an offset that has a structural relief-corrected separation that matches the thickness of the average stratigraphic unit thickness has a 50-percent chance of being seen and assume that structural relief-corrected slip that exceeds the thickest layer is certain to be seen (and that 0 offset has 0 chance of being seen). Use the frequency distribution of thicknesses to interpolate the probability between these estimates.

Multiply these probabilities times the spatial coverage factor to obtain an estimate of the probability of seeing different sized slip events at a trench site.

Although there are significant assumptions made and the entire approach is only semiquantitative, we believe it roughly captures the quality and likely completeness of the data derived from a paleoseismic site.

So far, we have focused on identifying the possibility of missing events. An equally important question is what is the chance that the record contains too many events. At issue is whether we should consider event chronologies a lower limit on earthquake recurrence if we always have some chance of missing events. Although it is difficult to prove with the limited data available, we believe that for sites with adequate coverage and resolution (as described

above), conducted by careful paleoseismologists, the number of missing events and extra events are likely to be similar. This means missing and overinterpreted cases contribute mainly to the amount of uncertainty but not to a systematic bias. For the UCERF3 Grand Inversion this means that the reported number of surface rupturing events can be used as the expected value for rate comparison purposes. One could argue (fig. I12) that at different stages of the investigation the bias could be on one side or the other, but it would be very difficult to assess, even qualitatively.

We also have not focused on the quality of event evidence. A number of workers have proposed approaches to assessing event quality (McCalpin, 1996; Scharer, 2005; , and informal discussions among paleoseismologists have explored the viability of a "paleoseismic index" to quantify the likelihood that a number of pieces of evidence indicated an earthquake. Such an "index" could easily be added to our framework but is beyond the scope of this appendix.
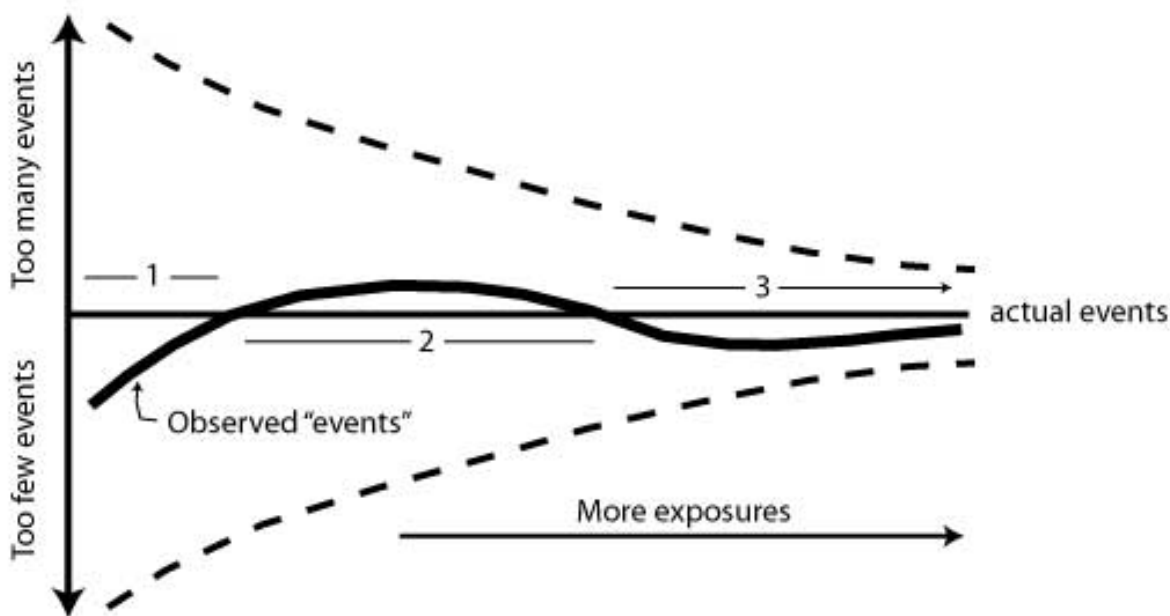

Figure I12. Schematic diagram of how the number of paleo-earthquakes that can be identified at a site (solid) and the uncertainty (dashed) varies with the number of exposures at a paleoseismic site. With a few exposures (stage 1 above) the uncertainty is large, and it is likely that more events are missed than extra false events are included because with a few exposures it is easy to miss evidence for events and hard to separate deformation that may be due to multiple events. Some false extra events are possible but will likely be outnumbered by missed events. As more exposures are studied (stage 2), especially as the exposures more fully cross the entire zone of deformation and cover a greater volume of deformed section along strike of the fault, the record is likely to be biased with too many events because the real events become better characterized; however, more exposures provide greater opportunity to misinterpret a feature, such as nontectonic features like burrows or tectonic features like upward terminations of fractures that don't clearly reach the paleo-event horizon. Finally, as study of the site develops to the point where the structure and stratigraphy are fully understood (stage 3), spurious "events" are removed. Although missing events may remain due to stratigraphic hiatuses, the observed number of paleo-earthquakes and the uncertainty should approach the actual number of resolvable events as the site study is completed.